# Self-diffusivity measurement of Eutectic $F^7$LiNaK with and without Additives using Quasi-elastic Neutron Scattering

G. S. Rakib, Shao-Chun Lee, Melissa Rose, Rebecca Mills, Daniel M. Pajerowski, Y Z, Brent J. Heuser*

**Abstract**

The atomic scale relaxation dynamics of eutectic $F^7$LiNaK (46.5 LiF-11.5 NaF-42 KF mol%, Li-7 enriched) were measured using quasi-elastic neutron scattering (QENS) over a temperature range of 500 to 750 ℃. The effect of adding 0.988 mol% cerium, 0.499 mol% cesium, and 1.21 mol% zirconium individually to the dynamics of $F^7$LiNaK was also investigated. The relaxation process in both pure and doped liquid $F^7$LiNaK salts was fit with a stretched exponential function and the temperature dependence follows an Arrhenius behavior over a wave vector transfer range of 0.4 $Å^{-1}$ < Q < 0.9 $Å^{-1}$. The measured activation energy for self-diffusion is $E_a = 0.77 \pm 0.02\ eV/atom$ for pure molten $F^7$LiNaK. The QENS response with additives added to $F^7$LiNaK was also fit with a stretched exponential and the associated Arrhenius behavior was characterized with activation energies of $E_a = 0.88 \pm 0.01\ eV/atom$ for zirconium (1.21 mol%), $E_a = 1.02 \pm 0.02\ eV/atom$ for cerium (0.988 mol%), and $E_a = 0.71 \pm 0.03\ eV/atom$ for cesium (0.499 mol%). The measured diffusivities are compared to those simulated with a neural network force field model by Lee *et al*. [J. Phys. Chem. B 125, 10562–10570. https://doi.org/10.1021/acs.jpcb.1c05608].

**Keywords:** QENS, FLiNaK, molten salt, additives, diffusivity, activation energy

## 1. Introduction:

Molten salt reactor (MSR) is one of the leading candidates of GEN-IV advanced reactors because of improved safety features and greater thermal efficiency.[1,2] MSRs employ molten salts as the low-pressure primary coolant or fueled coolant depending on the reactor design.[1,3] In some cases, such as the fluoride salt-cooled high-temperature reactor (FHR), molten salts are proposed as secondary coolant to extract heat due to their excellent heat transfer characteristics.[4] Beyond their applications in fission reactors, molten salts containing lithium and beryllium have breeding and cooling applications in fusion reactors.[5] Moreover, molten salts have utility in energy storage technology.[6] Despite these engineering applications, a comprehensive quantification of the thermophysical and transport properties of molten salts and the effect of additives on salt at high temperatures is still lacking. Understanding these properties is crucial for the MSR development as they directly influence the neutronics and thermal hydraulics.

Eutectic LiF-NaF-KF (46.5-11.5-42 molar %) has excellent characteristics for engineering applications and mimics certain properties of eutectic FLiBe such as density, viscosity, melting temperature, thermal expansion, thermal conductivity, and surface tension while eliminating the need to handle toxic beryllium.[7–9] Useful characteristics of eutectic FLiNaK such as low melting point, reasonable heat capacity, high boiling point, and good chemical stability at high temperature made this salt desirable in the MSR and concentrated solar energy (CSP) field.[10,11] Density, viscosity, thermal diffusivity, thermal conductivity, heat capacity, melting temperature, the heat of fusion measurements of FLiNaK have been reported. [12–17] However, these data are sporadic and have large variations.[18] In addition to addressing these data gaps, the deployment of molten salts in MSRs with fueled coolants necessitates a thorough understanding of how fission product, impurities from corrosion, and actinides affect the physiochemical properties of the salt.

In this work, we aim to employ advanced experimental tools, namely quasi-elastic neutron scattering (QENS), to fill some of the data gaps in FLiNaK thermophysical properties. QENS has a special feature that can be utilized to probe the atom-scale relaxation of molten salts as temperature changes.[19] This information helps to predict the equilibrium state of the molten salt. Additionally, the microscopic dynamics of molten salts, can be derived from the measured relaxation data, are important for understanding the bulk properties of the salt. For example, macroscopic transport properties like viscosity, diffusion, and thermal conductivity are influenced by the microscopic atomic dynamics.[20] Previous studies have mainly focused on the macroscopic (bulk) properties of FLiNaK and other molten salts.[7] However, the development of simulation tools for high-temperature molten salt systems requires microscopic experimental data both to understand the microscale phenomena and to validate the model outputs, which is currently scarce in this field. A better understanding of the atom scale phenomena would help the simulation models to generate more accurate macroscopic data.

As discussed earlier, quasi-elastic neutron scattering (QENS) is a useful technique for measuring diffusivity using neutron spectrometers. The current generation of neutron backscattering spectrometers in the U.S.[21,22] have optimized energy resolution applicable to slow dynamics in the timescale of nanoseconds.[23,24] The dynamics of liquids can be fast and require picosecond time scale measurements.[25] In this case, neutron spectrometers with a broader dynamic range are required. Neutron scattering based techniques are often sensitive to light elements and neighboring elements on the periodic table, can easily measure phonon modes, and can measure the diffusion dynamics via QENS. The self and collective dynamics study over broad time and length scales can shed light on the dynamic properties of molten FLiNaK.[25] We have employed incoherent scattering dominated QENS, which quantifies the dynamics without the interference effects associated with collective motions.

The existing FLiNaK diffusion data includes the self-diffusion coefficient of constituent species measured via the capillary reservoir technique within a temperature range spanning 480 to 663 ºC.[26] Molecular dynamics simulations using a neural network forcefield (NNFF) model have recently been performed by S. C. Lee *et al*.[27] They calculated the dynamics of individual species (Li, Na, K, and F) and thermophysical properties like density and viscosity. Another set of MD simulation has been performed separately by Galashev *et al.* and Zakiryanov reports the physiochemical properties of $CeF_3$-FLiNaK, $NdF_3$-FLiNaK melt and the dynamics of individual constituent species.[28–30]

In this work, the self-diffusivity of eutectic $F^7$LiNaK salt is measured with QENS over a temperature range of 500 to 750 ºC ($T_{melt}$ = 454 ºC for eutectic FLiNaK[31]). The methodology involves constructing an Arrhenius plot of the measured diffusivities to determine the activation energy for self-diffusion (diffusion in the absence of concentration gradients). This activation energy represents an elemental averaged quantity weighted by the incoherent macroscopic scattering cross section. The measured ionic self-diffusivity of FLiNaK is presented in contrast to previously reported FLiBe. Furthermore, the effect of adding individual cerium, cesium, and zirconium as fluoride additives at different concentrations on the pure $F^7$LiNaK diffusivities and activation energy is quantified and compared.

## 2. Materials and Methods

A eutectic mixture of $^7$LiF-NaF-KF (46.5-11.5-42 mol %) was synthesized at Argonne National Laboratory by procuring high-purity reagent $^7$LiF, NaF, and KF salts. The $^7$LiF precursor salt was 99.96% Li-7

enriched. Analysis of the synthesized salt used here has been published by Gardner *et al.* [31] The isotopic enrichment avoids the large neutron absorption of eutectic FLiNaK with natural abundance of Li-6. The precursor salts were mixed and underwent two melt-solidification cycles in the ANL glove box facilities (<5 ppm $O_2$ and <1 ppm $H_2O$). The reagents were placed in graphite crucibles and heated at 300 ºC for three hours to remove residual water prior to mixing and then heated to 700 ºC for three hours. The $^7$LiF and NaF were baked as single batches and the KF was baked in two batches. A single batch of F$^7$LiNaK was prepared by combining appropriate masses of dried reagent salts to achieve a composition of 46.7-11.3-42.0 mol % $^7$LiF-NaF-KF in a large graphite crucible. The batch was mechanically mixed and then melted at 700 ºC for 6 hours. The crucible was left in the furnace to cool slowly. The compositional analysis of prepared F$^7$LiNaK was performed using inductively coupled plasma-mass spectrometry (ICP-MS), inductively coupled plasma-optical emission spectrometry (ICP-OES), and x-ray diffraction.[31] The purities of the constituent metal fluoride salts are reported in the certificate as: $^7$LiF powder ≥ 99%, NaF ≥ 99.99%, KF≥ 99% based on trace metal analysis. Additives are purchased from chemical suppliers in the powder form of fluoride salts. The purities are reported in the certificate as: $CeF_3$ ≥ 99.9%, CsF ≥ 99.9%, and $ZrF_4$ ≥ 99.9% trace metal basis. The final sample preparation for the neutron scattering experiment was performed inside an argon glovebox at the University of Illinois Urbana-Champaign (UIUC) using the ANL synthesized F$^7$LiNaK, and the purchased individual additives. The vanadium sample containers (PAC006 cylindrical cans) were supplied from the Oak Ridge National Laboratory. These sample cans had titanium threaded lids. All samples were sealed under an argon environment and transported to the Oak Ridge National Laboratory Spallation Neutron Source (SNS) helium glovebox for storage. The sample mass information is provided in Table 1.

**Table 1.** F$^7$LiNaK and additive mass for each sample; individual additives are added in the form of $CeF_3$, CsF, and $ZrF_4$ compound to introduce cerium, cesium, and zirconium in the F$^7$LiNaK, respectively (mol %, total atom basis)

| **Sample** | **F$^7$LiNaK mass [g]** | **$CeF_3$/CsF/$ZrF_4$ mass [g]** | **mol% based on formula unit** |
|---|---|---|---|
| Pure F$^7$LiNaK | 2.9163 | - | - |
| F$^7$LiNaK + 0.988 mol % Ce | 2.6501 | 0.2600 | 2.015 |
| F$^7$LiNaK + 1.21 mol % Zr | 2.6513 | 0.2756 | 2.598 |
| F$^7$LiNaK + 0.499 mol % Cs | 2.8042 | 0.1041 | 0.9998 |

The QENS experiment was performed using the time-of-flight Cold Neutron Chopper Spectrometer (CNCS) at the SNS.[32] This is a high resolution, direct geometry disc chopper spectrometer with broad detector coverage. The QENS measurements reported here used an incident neutron energy of 3.32 meV in the high-flux mode. The static structure factor of molten F$^7$LiNaK at 500 ºC was measured with 12.0 meV incident neutrons. The energy resolution with 3.32 meV incident energy was approximately 110 μeV (FWHM) at the elastic line (ΔE = 0). The wavevector transfer range corresponding to this incident energy is 0.3 Å$^{-1}$ ≤ Q ≤ 2.3 Å$^{-1}$. Pure F$^7$LiNaK and Ce added samples were run without any gasket inside MICAS vacuum furnace. Cs and Zr samples had graphite gasket sealing to prevent any unwanted leakage inside the furnace environment during the experiment. The threaded lids were connected to the sample holder stick that aligns with the vertical centerline of the vacuum furnace. The temperature was measured with a thermocouple mounted close to the sample but not in the incident beam. Four temperature data has been

acquired for each $F^7$LiNaK sample: 500, 580, 670, and 750 ºC. Initial melting was confirmed by monitoring the diffraction with an incident neutron energy of 12.0 meV. The melting of cerium fluoride in FLiNaK was previously confirmed in a neutron diffraction measurement and no presence of cerium oxide was detected (see Figure S1 in supplementary).[18] We measured the resolution function with the sample in the incident beam upon cooling below 300 ºC so that no diffusive motions occurred. The data acquisition time ranged from three to five hours at each temperature.

The intensity measured in a QENS experiment comes from both incoherent and coherent scattering and can be expressed as Eqn. (1):

$$\frac{d^2\sigma}{dEd\Omega} = \frac{k_f}{4\pi k_i}[\sigma_{inc}\, S_{inc}(Q,E) + \sigma_{coh}\, S_{coh}(Q,E)] \quad (1)$$

where $k_i$ is the incident wavevector, $k_f$ is the scattered wavevector, $\sigma_{inc}$ and $\sigma_{coh}$ are the incoherent and coherent microscopic neutron scattering cross-sections, respectively. Uncorrelated diffusive motions broaden the incoherent dynamic structure factor. Similarly, collective diffusion motions broaden the coherent counterpart. The analysis of this broadening can unfold the diffusive dynamics on the microscopic scale.

Data fitting was performed over the measured energy range and for all Q-bins ~~of 0.4 Å$^{-1}$ < Q < 0.9 Å$^{-1}$ using four Q bins~~. However, we restricted our diffusivity analysis to a low Q range (0.4 Å$^{-1}$ < Q < 0.9 Å$^{-1}$) because other non-diffusive modes of ionic liquid motion build in at higher Q.[33] The resolution function can be expressed as a single Gaussian as shown in Eqn. (2),

$$\mathrm{R}(Q,E) = \frac{f(Q)}{\sigma(Q)\sqrt{2\pi}} e^{-\frac{1}{2}\left(\frac{E-\bar{E}(Q)}{\sigma}\right)^2} \quad (2)$$

where $f(Q)$, $\sigma(Q)$, and $\bar{E}(Q)$ represent the intensity, width, and mean value of the gaussian profile. The incoherent dynamic structure factor can be written as Eqn. (3),

$$S_{inc}(Q,E) = A(Q)\{f_{elastic}(Q)R(Q,E) + [1 - f_{elastic}(Q)]S'(Q,E)\} + bkg(Q) \quad (3)$$

where $A(Q)$ is an amplitude factor, $f_{elastic}(Q)$ represents the fraction of scattering that is within the instrumental resolution function $R(Q,E)$, $bkg(Q)$ is the background, and $S'(Q,E)$ represents the QENS response. We note true elastic scattering ($\Delta E = 0$) is not possible from a liquid and $f_{elastic}(Q)$ captures the scattered intensity with small energy change that falls within the 110 μeV instrumental resolution at 3.32 meV incident energy. The QENS response is given by Eqn. (4),

$$S'(Q,E) = \mathcal{F}\{\mathcal{F}^{-1}\{R(Q,E)\}F(Q,t)\} \quad (4)$$

where $\mathcal{F}\{\cdots\}$ represents a Fourier transform and $F(Q,t)$ is the intermediate scattering function, which we assume *a priori* is a stretched exponential function as Eqn. (5),

$$F(Q,t) = e^{-\left[\frac{t}{\tau(Q)}\right]^{\beta(Q)}} \quad (5)$$

where $\tau(Q)$ is the decay constant and $\beta(Q)$ is the stretching exponent. The stretched exponential function is also known as the Kohlrausch–Williams–Watts (KWW) function.[34] This stretched exponential feature

is shown later to be a good approximation, which in our case reflects a heterogeneous distribution of self-diffusivities of each constituent element in the system. The background term includes fast dynamic processes associated with the atomic vibrational spectra which have a very broad inelastic or quasi-elastic scattering response in the energy domain associated with QENS.

The microscopic and macroscopic cross sections of the $F^7$LiNaK constituents are listed in *Table 2*. Macroscopic cross sections are calculated using a molten $F^7$LiNaK density of $\rho$ = 2.165 g/cm$^3$ at 500 ºC.[15] The total coherent scattering cross section is larger than the incoherent scattering cross section. However, the diffusivity we determine from the QENS response still represents the self-diffusivity for two reasons. First, in the Q-range we studied (0.4 Å$^{-1}$ < Q < 0.9 Å$^{-1}$), the coherent scattering is suppressed by the structure factor. The primary structure factor peak of $F^7$LiNaK is at $Q_{max}$ ~2.5 Å$^{-1}$. [35,36] At Q values much less than this $Q_{max}$, the buildup of structural coherence is not significant. Second, the collective diffusion coefficient from coherent scattering is about the same value as the self-diffusion coefficient in the multi-component liquid mixtures because of elemental fluctuations.[19,37]

**Table 2.** Coherent and incoherent thermal neutron scattering cross sections for the $F^7$LiNaK constituent elements.[38]

| Element | molar % | $\sigma_{inc}$ [$barns$] | $\sigma_{coh}$ [$barns$] | $\Sigma_{inc}$ [$10^{-2}\ cm^{-1}$] | $\Sigma_{coh}$ [$10^{-2}\ cm^{-1}$] |
|---|---|---|---|---|---|
| F | 1.00 | 0.0008 | 4.017 | 5.05 ×10$^{-3}$ | 25.4 |
| Li-7 | 0.47 | 0.78 | 0.619 | 2.29 | 1.82 |
| Na | 0.11 | 1.62 | 1.66 | 1.18 | 1.2 |
| K | 0.42 | 0.27 | 1.69 | 0.72 | 4.48 |
| Ce | 0.00988 | 0.001 | 2.94 | 6.23 ×10$^{-5}$ | 0.18 |
| Cs | 0.00499 | 0.21 | 3.69 | 6.61 ×10$^{-3}$ | 0.12 |
| Zr | 0.01207 | 0.02 | 6.44 | 1.52 ×10$^{-3}$ | 0.49 |

## 3. Results and Discussions

The kinematic Q-E space from pure $F^7$LiNaK for the 3.32 meV incident neutron energy is shown in Figure 1a. The fitting employed here uses Eqn. (3) to fit the data in the energy domain by performing the Fourier transforms associated with Eqn. (4) with the measured resolution function and Eqn. (5). This procedure includes many correlated fitting parameters, a non-ideal situation. We performed preliminary fits of all recorded Q-bins over the measured energy range ~~(not shown)~~ and observed the background for a given sample did not vary significantly with Q or temperature. We therefore fixed the background for each sample at a level determined in the preliminary fits (5x10$^{-4}$ for all samples, Q bins, and temperatures). The stretching exponent exhibited fluctuations about $\beta$ = 0.4 after the background was fixed and shown in Figure 1b. We therefore fixed $\beta$ = 0.4 for all samples, Q bins, and temperatures in the following step. We note that the fitting was insensitive to a slightly higher or lower beta value. We observed the $f_{elastic}$ behavior shown in Figure 1c after the background and beta were fixed. This Q and temperature dependent

$f_{elastic}$ presented in Figure 1c is for pure $F^7$LiNaK. The final fit of each QENS measurement was performed by allowing $\tau$ to vary with Q and temperature while keeping the background at $5x10^{-4}$, $\beta$ at 0.4, and $f_{elastic}$ fixed at the values shown in Figure 1c. Only the Q bins in the 0.4 $Å^{-1}$ < Q < 0.9 $Å^{-1}$ range were used for the diffusivity calculation. The fitting parameter $\beta$, background, and the $f_{elastic}$, all have arbitrary units.

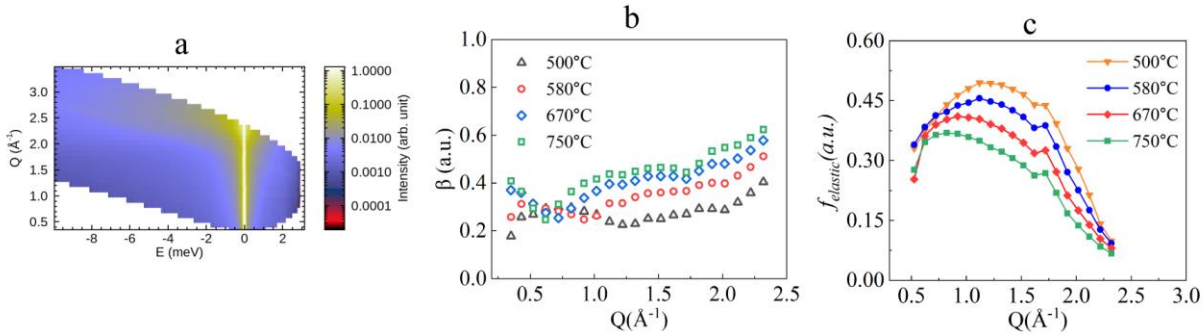


**Figure 1.** (a) Scattering intensity from pure $F^7$LiNaK sample at 500 ºC, probed with 3.32 meV incident energy neutrons in Q-E space (b) stretching exponent behavior for pure $F^7$LiNaK upon setting the constant background to $5x10^{-4}$ for all Q and temperature (c) $f_{elastic}$ $(Q)$ dependence of pure $F^7$LiNaK on temperature.

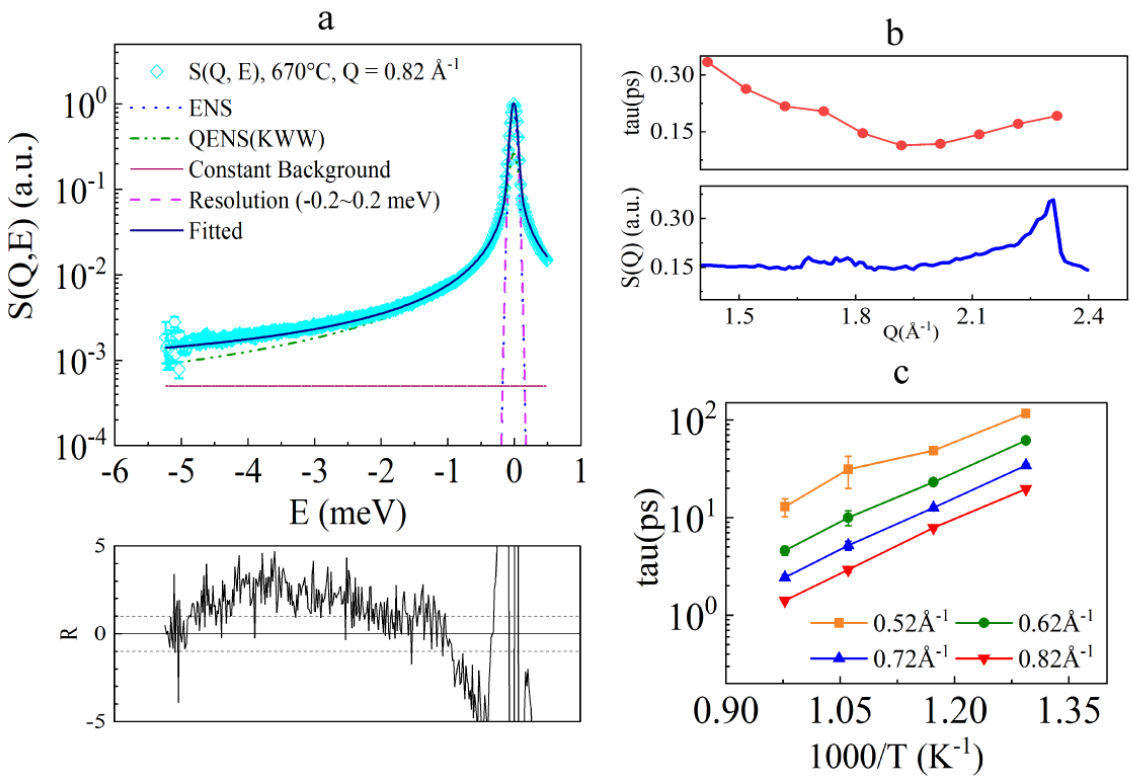


**Figure 2.** (a) Fitted experimental scattering intensity for Q = 0.82 $Å^{-1}$ at 670 ºC in the energy domain for pure $F^7$LiNaK. The residual between the fit and data is shown as well and defined as, R = (data-fit)/error; (b) The relaxation time becomes longer as the scattering intensity reaches to the maximum at Q = 2.3 $Å^{-1}$,

rendering to de Gennes narrowing for $F^7$LiNaK at T(670 ºC) > $T_{melt}$; (c) Relaxation time τ (ps) plotted versus 1000/T.

A representative fit of Q = 0.82 $Å^{-1}$ at 670 ºC for pure $F^7$LiNaK is shown in Figure 2a with the contributions from all fitting components shown. We observed a slowing down in the dynamics at Q = 2.3 $Å^{-1}$ where the total scattering intensity $S(Q,E)$ becomes maximum, as shown in Figure 2b. This is consistent with the de Gennes narrowing phenomenon for complex liquid.[39] Figure 2c shows the relaxation time $\tau(Q)$ extracted from the fitting of the intermediate scattering function $F(Q,t)$ as a function of inverse temperature. This variation follows an Arrhenius response analyzed below.

Additional representative data fitting for pure $F^7$LiNaK is shown in Figure 3. We fit the QENS response associated with neutron energy gain (which by convention is E<0 in Figure 2 and Figure 3) because energy loss cannot be greater than the incident neutron energy (3.32 meV here) and this constraint significantly reduces the dynamic range we can analyze. Greater neutron energy gain range occurs at higher Q due to the kinematics associated with inelastic scattering (as shown in Figure *1*a). Larger QENS broadening associated with greater diffusivity with temperature is observed in Figure *3*b.

The QENS response for regular bulk diffusion follows a $\tau \propto Q^{-2}$ relation at low Q.[40] The KWW model can be interpreted as the superposition of different simple exponential relaxations with $\beta = 1$ or a single non-exponent ($\beta \neq 1$) relaxation.[19,41] The mean relaxation time can be calculated according to Eqn. (6),

$$\langle \tau \rangle = \int_0^\infty F(Q,t)dt = \frac{\tau}{\beta}\Gamma\left(\frac{1}{\beta}\right) \tag{6}$$

where $\Gamma(x)$ is the gamma function. Eqn. (5) is used to get the intermediate scattering function with $\beta = 0.4$. The mean relaxation time is related to the diffusion coefficient *D* via the Gaussian approximation $\langle \tau \rangle^{-1} = DQ^2$. The Gaussian approximation is only valid in the hydrodynamic limit at low Q, where the characteristic length scale is large and the QENS response is independent of specific diffusive random motions over atomic length scales associated with Brownian motion.

Least squares fits of the Q dependence of the mean relaxation time using the Gaussian approximation give the diffusivity from the best fit slope. These diffusivities can be used to construct an Arrhenius plot. The diffusivity is measured as diffusion coefficient *D* and given by Eqn. (7),

$$D(E_a,T) = D_0 e^{-\frac{E_a}{kT}} \tag{7}$$

where $E_a$ is the activation energy, *k* is the Boltzmann constant, and $D_0$ is the diffusion constant.

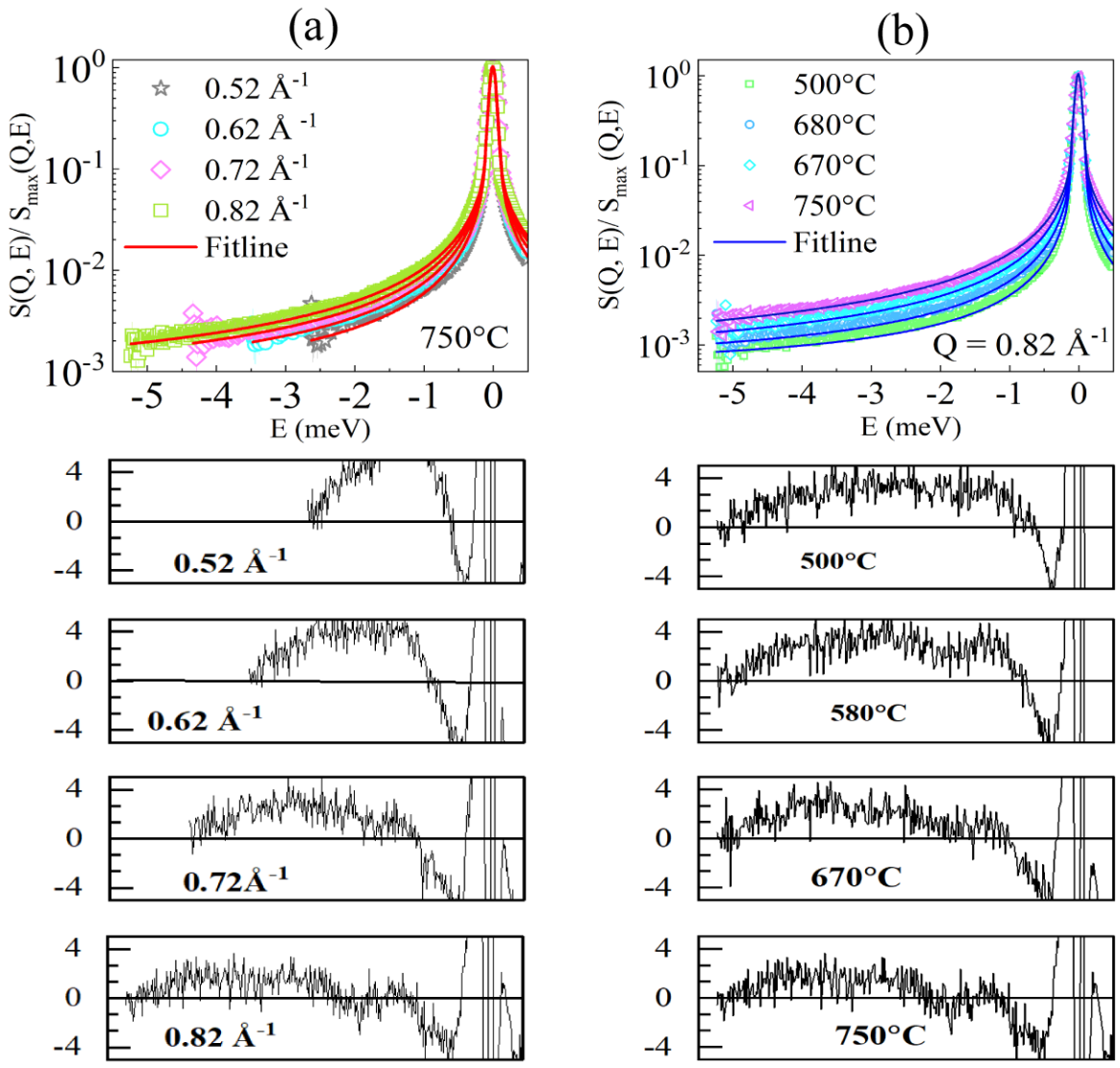


**Figure 3.** (a) Normalized scattering intensity of pure $F^7LiNaK$ at T=750 ºC for different Q bins in the low Q range; (b) normalized intensity of pure $F^7LiNaK$ for Q = 0.82 Å$^{-1}$ for all temperatures. A convention of negative energy for neutron energy gain is used for direct geometry time of flight inelastic spectrometers such as the CNCS. The fitting residual are shown below each primary figure.

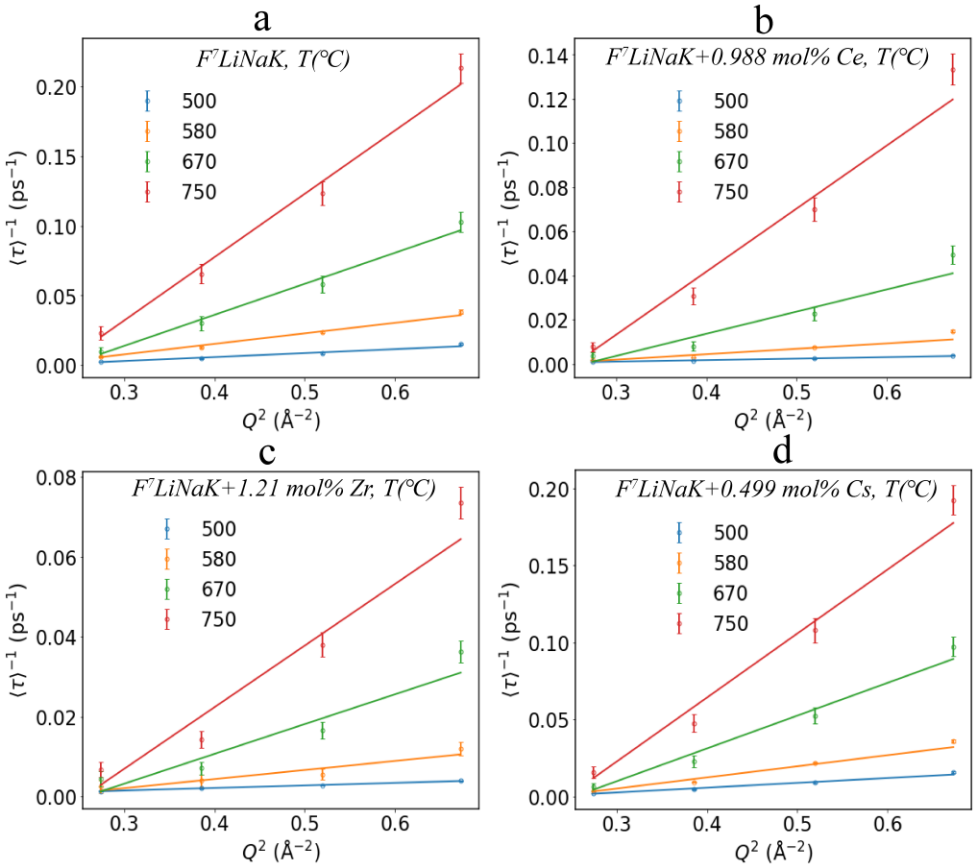


**Figure 4.** Fit of the Gaussian approximation to the $Q^2$ dependence of the mean relaxation time. The slope of the linear error weighted fitting gives the self-diffusivity at each temperature; (a) pure $F^7$LiNaK (b) $F^7$LiNaK with 0.988 mol% Ce (c) $F^7$LiNaK with 1.21 mol% Zr (d) $F^7$LiNaK with 0.499 mol% Cs.

The best fits to the $\langle\tau\rangle^{-1} - Q^2$ behavior are shown in Figure 4 a-d. An Arrhenius plot that includes all samples is shown in Figure 5 and the activation energies from the best fits are tabulated in Table 3. The addition of cerium and zirconium increases the activation energy while lowering the diffusivity over the measured temperature range. The decrease in diffusion can be attributed to the heavier mass of the additives and their formation of fluoride complex structures in the medium (e.g. $ZrF_6^{2-}, ZrF_7^{3-}$). Cerium and zirconium cations can capture multiple $F^-$ ions to form complex ionic structures due to the electrostatic interactions.[42–44] Furthermore, small individual complex ions might bond via edge or corner sharing to form chains at higher additive concentrations in the melt.[43,45] It is found that the self-diffusion of species is correlated to the ion pair breaking rates, indicating the presence of such bound complexes affects mass transport in molten salts.[46]

The in-silico study by Zakiryanov (2023) discussed about the presence of moderately stable $[CeF_x]^{3-x}$ groupings in the FLiNaK-$CeF_3$ system and the impact on the physicochemical properties.[30] This study, along with another independent MD study by Galashev *et al.* reported a decrease in the mobility of the positive ions with increasing atomic mass and showed cerium has the lowest mobility and largest activation energy (shown in Table 4 ) in the FLiNaK-$CeF_3$ system.

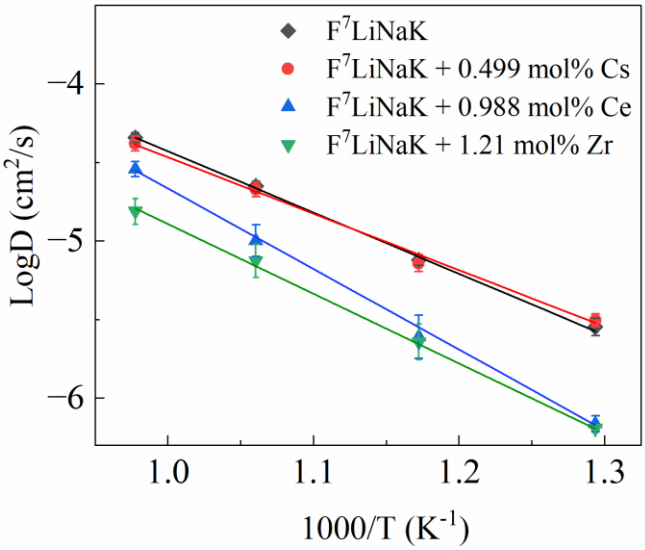


**Figure 5.** Arrhenius plots for pure eutectic $F^7$LiNaK and $F^7$LiNaK with 0.499 mol% Cs, 0.988 mol% Ce, and 1.21 mol% Zr. The best fit slope is proportional to the activation energy and the y-intercept is the diffusion constant, $D_0$.

**Table 3.** Activation energy (eV/atom) and diffusion constant for pure $F^7$LiNaK and $F^7$LiNaK with individual 0.988 mol% Ce, 0.499 mol% Cs and 1.21 mol% Zr additives.

| **$F^7$LiNaK samples** | **Activation Energy (eV/atom)** | **Diffusion constant, $D_0$ ($cm^2/s$)** |
|---|---|---|
| Pure $F^7$LiNaK | 0.77 ± 0.02 | 0.29 ± 0.17 |
| $F^7$LiNaK with 0.988 mol% Ce | 1.02 ± 0.02 | 2.88 ± 0.01 |
| $F^7$LiNaK with 1.21 mol% Zr | 0.88 ± 0.01 | 0.35 ± 0.10 |
| $F^7$LiNaK with 0.499 mol% Cs | 0.71 ± 0.03 | 0.13 ± 0.55 |

Zakiryanov (2023) also measured the mean lifetime of the Ce-F bond in FLiNaK at different temperatures, for three $CeF_3$ concentrations (5, 10, and 15 mol%). The study found that the mean lifetime of the Ce-F bond decreases by about one-third as the temperature increases from 950 to 1200 K [30]. This decrease in the Ce-F mean bond lifetime shows that the cerium complexes becomes unstable at higher temperatures. As a result, cerium diffusivity noticeably increases at high temperatures, as seen in Figure 6(b) and in our QENS results in Figure 5. In contrast, stable zirconium complexes and their chains were identified even at high temperatures (1273K)[45,47]. This indicates the diffusivity of zirconium to be less sensitive to temperature rise, unlike cerium. Therefore, our QENS results show a gradual increase in the diffusivity of the zirconium added FLiNaK sample with temperature and a lower activation energy as compared to the cerium sample.

The addition of cesium has little to no effect on the diffusivity of pure $F^7$LiNaK. The $Cs^+$ cation has a lower oxidation state (+1) compared to cerium or zirconium and this likely inhibits complex structure formation in the ionic molten salt. The local structure study of NaF-CsF molten salt using nuclear magnetic resonance (NMR) supports this statement. [48,49] The chemical shift of $^{19}F$ NMR peaks as a function of CsF concentrations obeys a linear relation, indicating the absence of long-lived cesium complexes in the NaF-

CsF melt. [48,50,51] In contrast, a non-linear correlation is observed due to the presence of bound fluorines (e.g., individual or bridged fluoride complexes) in NaF-$LaF_3$ and NaF-$AlF_3$ melt. Furthermore, the lower molar concentration of cesium might contribute to the lack of noticeable change in diffusivity. Our findings also suggest the investigation of complex structures formation in FLiNaK in the presence of various additives (for example, fission products) could influence the concentration of free $F^-$anions in salt. The activity of free $F^-$ is described by the term 'fluoroacidity' in literature and studies indicated this term to be related with molten salt corrosion. [43,52,53] Fluoroacidity can also be related to the transport of the species in a molten salt. [54,55] For instance, a qualitative comparison between the self-diffusivity of FLiNaK, and FLiBe can be made in relation to fluoroacidity. FLiNaK, being fully dissociated, has higher free $F^-$concentration and thus it is fluorobasic in nature[55]. The constituent ions being relatively free, the mobility of ions is expected to be unrestricted. However, the formation of beryllium fluoride complexes ($BeF_4^{2-}$, $Be_2F_7^{3-}$, and the chain formation among them via edge sharing) in FLiBe binds the free fluorines, and the mobility of the beryllium and fluorine ions becomes restricted due to the enhanced effective mass of such complexes.[56] The slowing down of the beryllium and fluorine ionic mobility has been observed in the study of FLiBe using a machine learned potential based MD simulation by Alejandro *et al.*[56] The result is shown in Figure *6*(a) in comparison to FLiNaK. It is noticeable from the figure that the diffusivity of beryllium and fluorine in FLiBe is lower than the FLiNaK due to the complex formation. Thus, a fluorobasic salt might be more likely to see a higher ionic self-diffusivity as compared to a fluroacidic salt, given there are formation of complexes.

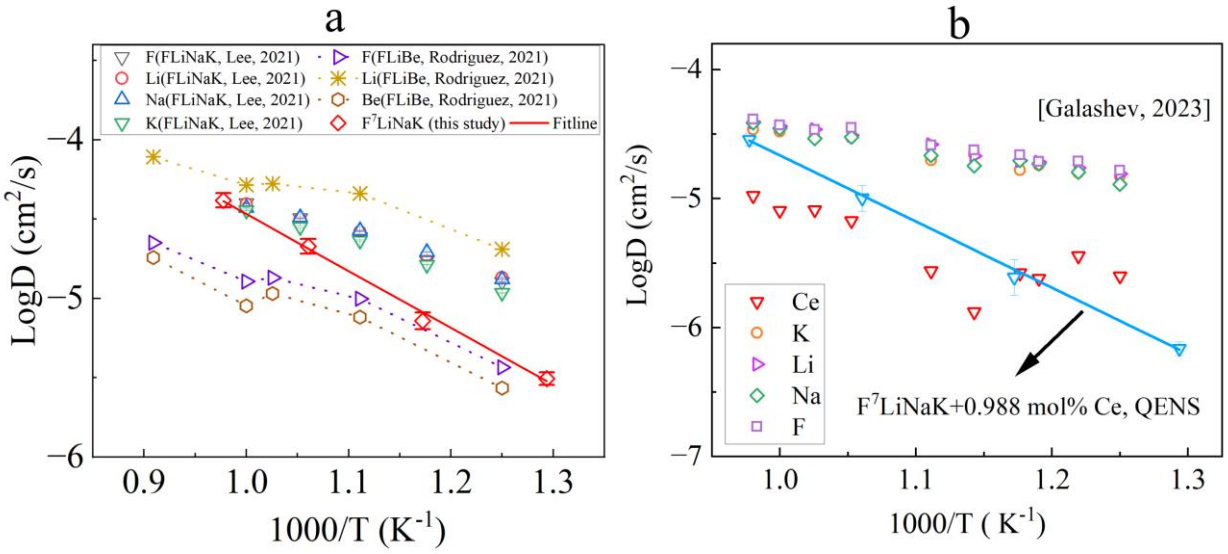


**Figure 6.** (a) Pure $F^7$LiNaK self-diffusivity from QENS measurements compared to the elemental diffusivities of the FLiNaK constituents calculated from the first principle NNFF model[27], and FLiBe constituents calculated from machine learning potential (MLP) MD [56]; (b) Elemental diffusivities of 0.85 FLiNaK-0.15 $CeF_3$ constituents measured from *ab initio* MD simulation [28] as compared to the 0.988 mol% Ce + $F^7$LiNaK diffusivity from QENS measurement (this study). Error bars were not reported in those literature studies.

The elemental diffusivities of FLiNaK constituents (F, Li, Na, K) shown in Figure 6a are calculated from the first principle calculation using the machine learned neural network force field (NNFF) model by Lee *et al.* [27] This study found that the calculated ionic self-diffusivity was within the error bar limit of the measured self-diffusivity of FLiNaK by Umesaki *et al.*[26] A comparison between those elemental

diffusivities and the pure $F^7$LiNaK diffusivity measured from this experiment is shown in Figure 6a. There are noticeable differences between the calculated elemental $F^7$LiNaK diffusivities of Lee *et al.* and our measured self-diffusivities. There are several possible reasons for this difference. First, the NNFF model was trained against a first principal simulation of the static FLiNaK structure. Subsequent molecular dynamics simulations using the NNFF model were used to determine the constituent diffusivities based on mean squared displacements. It is possible this protocol does not correctly capture mass transport. Second, Lee *et al.* did not perform the weighting associated with incoherent neutron scattering for a direct comparison with the QENS self-diffusivities. Finally, our protocol used to fit the QENS data could introduce systematic errors. However, we attempted various alternative strategies and did not observe deviations that account for the differences seen in Figure 6a. Therefore, we believe the measured self-diffusivities for pure $F^7$LiNaK and $F^7$LiNaK with additives using QENS are trustworthy.

In addition, a higher lithium self-diffusivity in FLiBe is noticeable from Figure 6a than in FLiNaK. This might be related to factors such as the density difference of the two salts at the same temperature, the abundance of free fluorines, and different forcefield used in the simulations.

We also show the comparison of elemental diffusivities in presence of cerium in the liquid found from MD simulation by Galashev *et al.* [28] to our neutron scattering results in Figure 6b. Here the agreement is better although the MD results have significant scatter and do not follow a linear or Arrhenius behavior. The error bars were not available for the Galashev *et al.* data set, hence the linear fitting of diffusivities is not error weighted in Table 4. Finally an *in silico* study reported the elemental activation energy of FLiNaK- $CeF_3$ at different concentrations [30]; this is also included in Table 4.

**Table 4.** Activation energy [$E_a$ (eV/atom)] measured from different experiments and simulations for pure FLiNaK and FLiNaK-$CeF_3$ melt constituents.

| Elements | **Pure FLiNaK** [experiment][26] | **Pure FLiNaK** [MD NNFF][27] | **0.05$CeF_3$-0.95FLiNaK** [*in silico* MD][30] | **0.10$CeF_3$-0.9FLiNaK** [*in silico* MD][30] | **0.15$CeF_3$-0.85FLiNaK** [*in silico* MD][30] | **0.15$CeF_3$-0.85FLiNaK** [*ab initio* MD][28] |
|---|---|---|---|---|---|---|
| F | 0.32± 0.07 | 0.40± 0.01 | 0.39 | 0.39 | 0.42 | 0.28 ±0.01 |
| Li | 0.39 ± 0.04 | 0.37± 0.01 | 0.37 | 0.38 | 0.42 | 0.30 ± 0.01 |
| K | 0.33±0.08 | 0.41± 0.02 | 0.35 | 0.36 | 0.40 | 0.28 ±0.02 |
| Na | 0.38 ± 0.07 | 0.39± 0.03 | 0.39 | 0.36 | 0.43 | 0.32 ± 0.02 |
| Ce | | | 0.41 | 0.46 | 0.51 | 0.49 ± 0.13 |
| Pure $F^7$LiNaK (this work) | | | 0.77 ± 0.02 | | | |
| $F^7$LiNaK + 0.988 mol% Ce (this work) | | | 1.02 ± 0.02 | | | |
| $F^7$LiNaK + 1.21 mol% Zr (this work) | | | 0.88 ± 0.01 | | | |
| $F^7$LiNaK + 0.499 mol % Cs (this work) | | | 0.71 ± 0.03 | | | |

## 3. Conclusions

The introduction of such fission products in molten salts will induce the formation of complex structures or small chains depending on the electrochemical conditions that influence the physicochemical properties of the system. In our work, the self-diffusivity of pure $F^7$LiNaK and $F^7$LiNaK with Ce, Cs, and Zr additives

were measured between 500 to 750 ºC using QENS at the SNS at ORNL. The addition of Ce and Zr additives impedes dynamical mass transport. This is reflected by smaller diffusivities and larger activation energies relative to pure $F^7$LiNaK molten salt. Cesium has little effect on self-diffusivity compared to pure $F^7$LiNaK, an effect attributed to the lower (+1) valence state of this cation.

## Author Information

### Corresponding Author

**Brent J. Heuser**- Nuclear, Plasma and Radiological Engineering, University of Illinois, Urbana, IL-61801, https://orcid.org/0000-0002-8283-5209, email: bheuser@illinois.edu

### Authors

**G. S. Rakib**- Nuclear, Plasma and Radiological Engineering, University of Illinois at Urbana- Champaign, Urbana, IL-61801, United States, https://orcid.org/0000-0003-1307-0668

**Shao-Chun Lee** - Department of Nuclear, Plasma, and Radiological Engineering, University of Illinois at Urbana−Champaign, Urbana, Illinois 61801, United States; https://orcid.org/0000-0002-0665-5337

**Melissa Rose** - Chemical & Fuel Cycle Technologies Division, Argonne National Laboratory, Argonne, IL 60439, United States

**Rebecca Mills** – Neutron Scattering Division, Oak Ridge National Laboratory, Oak Ridge, TN 37830, United States

**D. M. Pajerowski-** Neutron Scattering Division, Oak Ridge National Laboratory, Oak Ridge, TN 37830, United States; https://orcid.org/w0000-0003-3890-2379

**Y Z** - Department of Nuclear Engineering and Radiological Sciences, Department of Materials Science and Engineering, Department of Robotics, and Applied Physics Program, University of Michigan, Ann Arbor, Michigan 48105, USA; https://orcid.org/0000-0002-7339-8342

### CRediT Statement

**G S Rakib**: Investigation (lead); Data curation (lead); Visualization (lead); Formal analysis (lead); Writing- original draft (lead); Conceptualization (supporting). **S.-C. Lee**: Software (lead); Formal analysis (supporting); Writing- original draft (supporting). **Melissa Rose**: Resources; Writing-review and editing (equal). **Rebecca Mills**: Resources; Writing-review and editing (equal). **D. M. Pajerowski**: Resources; Writing-review and editing (equal). **Y Z**: Funding acquisition; Conceptualization; Writing- review and editing (equal). **Brent J. Heuser**: Supervision; Conceptualization; Resources; Writing- original draft (supporting), review and editing (equal).

### Notes

The authors declare no competing financial interest.

### Acknowledgements

This work is supported by the U.S. Department of Energy, Office of Nuclear Energy's Nuclear Energy University Programs, under Award Number DE-NE-0008884. A portion of this research used resources at the Spallation Neutron Source, a DOE Office of Science User Facility operated by the Oak Ridge National

Laboratory. Another portion of this research used resources of Chemical & Fuel Cycle Technologies Division at Argonne National Laboratory and was supported by the U.S. Department of Energy, Office of Nuclear Energy, under Contract DE-AC02-06CH11357.

## References

(1) Serp, J.; Allibert, M.; Beneš, O.; Delpech, S.; Feynberg, O.; Ghetta, V.; Heuer, D.; Holcomb, D.; Ignatiev, V.; Kloosterman, J. L.; Luzzi, L.; Merle-Lucotte, E.; Uhlíř, J.; Yoshioka, R.; Zhimin, D. The Molten Salt Reactor (MSR) in Generation IV: Overview and Perspectives. *Prog. Nucl. Energy* **2014**, *77*, 308–319. https://doi.org/10.1016/j.pnucene.2014.02.014.

(2) Ahmed, F.; Ara, N.; Deshpande, V.; Mollah, A. S.; Bhowmik, P. K. CFD Validation with Optimized Mesh Using Benchmarking Data of Pebble-Bed High-Temperature Reactor. *Prog. Nucl. Energy* **2021**, *134*, 103653. https://doi.org/10.1016/j.pnucene.2021.103653.

(3) Malik, M.; Chen, J.; Fulvio, A.; Brooks, C.; Grunloh, T. Uncoupled DEM Simulation to Investigate the Impact of Coolant Flow on Pebble Flow in Pebble Bed Reactor. In *20th International Topical Meeting on Nuclear Reactor Thermal Hydraulics (NURETH-20)*; American Nuclear Society: Washington, D.C., 2023; pp 3238–3251. https://doi.org/10.13182/NURETH20-40321.

(4) Romatoski, R. R.; Hu, L. W. Fluoride Salt Coolant Properties for Nuclear Reactor Applications: A Review. *Ann. Nucl. Energy* **2017**, *109*, 635–647. https://doi.org/10.1016/j.anucene.2017.05.036.

(5) Sagara, A.; Yamanishi, H.; Imagawa, S.; Muroga, T.; Uda, T.; Noda, T.; Takahashi, S.; Fukumoto, K.; Yamamoto, T.; Matsui, H.; Kohyama, A.; Hasizume, H.; Toda, S.; Shimizu, A.; Suzuki, A.; Hosoya, Y.; Tanaka, S.; Terai, T.; Sze, D.-K.; Motojima, O. Design and Development of the Flibe Blanket for Helical-Type Fusion Reactor FFHR. *Fusion Eng. Des.* **2000**, *49–50*, 661–666. https://doi.org/10.1016/S0920-3796(00)00360-4.

(6) Boretti, A.; Castelletto, S. The Perspective of Thermochemical Cycles for Concentrated Solar Energy. *ACS Appl. Energy Mater.* **2023**, *6* (22), 11420–11428. https://doi.org/10.1021/acsaem.3c01718.

(7) Janz, G. J.; Tomkins, R. P. T.; Allen, C. B. Molten Salts: Volume 4, Part 4 Mixed Halide Melts Electrical Conductance, Density, Viscosity, and Surface Tension Data. *J. Phys. Chem. Ref. Data* **1979**, *8* (1), 125–302. https://doi.org/10.1063/1.555590.

(8) Manohar S. Sohal; Matthias A. Ebner; Piyush Sabharwall; Phil Sharpe. *Engineering Database of Liquid Salt Thermophysical and Thermochemical Properties*; INL/EXT-10-18297, 980801; 2010; p INL/EXT-10-18297, 980801. https://doi.org/10.2172/980801.

(9) Rakib, G. S.; Lee, S. C.; Rose, M. A.; Pajerowski, D. M.; Heuser, B. J. Measurement of the Self-Diffusivity of Eutectic F7LiNaK Using Quasi-Elastic Neutron Scattering. *Trans. Am. Nucl. Soc.* **2023**, *128*, 365–367. https://doi.org/10.13182/T128-41919.

(10) Rose, M.; Wu, E.; Williamson, M. *Thermophysical Property Measurements: Improved Density, Viscosity and Thermal Diffusivity Methods*; ANL/CFCT--20/38, 1734862, 164442; 2020; p ANL/CFCT--20/38, 1734862, 164442. https://doi.org/10.2172/1734862.

(11) Sankar, K. M.; Singh, P. M. Effect of Oxide Impurities on the Corrosion Behavior of Structural Materials in Molten LiF-NaF-KF. *Corros. Sci.* **2022**, *206*, 110473. https://doi.org/10.1016/j.corsci.2022.110473.

(12) Cohen, S.; Jones, T. *A Summary of Density Measurements on Molten Fluoride Mixtures and a Correlation for Predicting Densities of Fluoride Mixtures*; ORNL-1702, 4334794; 1954; p ORNL-1702, 4334794. https://doi.org/10.2172/4334794.

(13) Khokhlov, V.; Korzun, I.; Dokutovich, V.; Filatov, E. Heat Capacity and Thermal Conductivity of Molten Ternary Lithium, Sodium, Potassium, and Zirconium Fluorides Mixtures. *J. Nucl. Mater.* **2011**, *410* (1–3), 32–38. https://doi.org/10.1016/j.jnucmat.2010.12.306.

(14) Lichtenstein, T.; Rose, M.; Krueger, J.; Wu, E.; Williamson, M. *Thermochemical Property Measurements of FLiNaK and FLiBe in FY 2020*; ANL/CFCT--20/37, 1734856, 164486; 2020; p ANL/CFCT--20/37, 1734856, 164486. https://doi.org/10.2172/1734856.
(15) Powers, W. D.; Cohen, S. I.; Greene, N. D. Physical Properties of Molten Reactor Fuels and Coolants. *Nucl. Sci. Eng.* **1963**, *17* (2), 200–211. https://doi.org/10.13182/NSE63-5.
(16) Rogers, D. J.; Yoko, T.; Janz, G. J. Fusion Properties and Heat Capacities of the Eutectic Lithium Fluoride-Sodium Fluoride-Potassium Fluoride Melt. *J. Chem. Eng. Data* **1982**, *27* (3), 366–367. https://doi.org/10.1021/je00029a041.
(17) Schorne-Pinto, J.; Aziziha, M.; Tisdale, H. B.; Mofrad, A. M.; Birri, A.; Christian, M. S.; Ard, J. C.; Booth, R. E.; Yingling, J. A.; Soldan Palma, J. P.; Dixon, C.; Loye, H.-C. zur; Besmann, T. M. Thermal Property Modeling and Assessment of the Physical Properties of FLiNaK. *ACS Appl. Energy Mater.* **2024**. https://doi.org/10.1021/acsaem.4c00321.
(18) Rakib, G. S.; Lee, S. C.; Rose, M. A.; Neuefeind, J. C.; Heuser, B. J. Measurement of the Pair Distribution Function of Molten Eutectic F7LiNaK Using Neutron Diffraction. *Trans. Am. Nucl. Soc.* **2023**, *128*, 368–370. https://doi.org/10.13182/T128-42095.
(19) Luo, P.; Jaiswal, A.; Zhai, Y.; Cai, Z.; Walter, N. P.; Zhou, L.; Ding, D.; Liu, M.; Mills, R.; Podlesynak, A.; Ehlers, G.; Faraone, A.; Bai, H.; Wang, W.; Z, Y. Atomic Dynamics of Metallic Glass Melts La 50 Ni 15 Al 35 and Ce 70 Cu 19 Al 11 Studied by Quasielastic Neutron Scattering. *Phys. Rev. B* **2021**, *103* (22), 224104. https://doi.org/10.1103/PhysRevB.103.224104.
(20) Demmel, F.; Mukhopadhyay, S. Quasielastic Neutron Scattering Measurements and *Ab Initio* MD-Simulations on Single Ion Motions in Molten NaF. *J. Chem. Phys.* **2016**, *144* (1), 014503. https://doi.org/10.1063/1.4939072.
(21) Dimeo, R. M.; Chowdhuri, Z.; Meyer, A.; Gehring, P. M.; Neumann, D. A. The NIST High-Flux Backscattering Spectrometer. *Appl. Phys. Mater. Sci. Process.* **2002**, *74* (0), s311–s313. https://doi.org/10.1007/s003390201605.
(22) Mamontov, E.; Zamponi, M.; Hammons, S.; Keener, W. S.; Hagen, M.; Herwig, K. W. BASIS: A New Backscattering Spectrometer at the SNS. *Neutron News* **2008**, *19* (3), 22–24. https://doi.org/10.1080/10448630802210578.
(23) Heuser, B. J.; Prisk, T. R.; Lin, J.; Dax, T. J.; Zhang, Y. Direct Measurement of Hydrogen Diffusivity and Solubility Limits in Zircaloy 2 (Formula Unit of ZrH0.0155) Using Incoherent Quasi-Elastic Neutron Scattering. *J. Nucl. Mater.* **2019**, *518*, 177–189. https://doi.org/10.1016/j.jnucmat.2019.02.045.
(24) Heuser, B. J.; Trinkle, D. R.; Jalarvo, N.; Serio, J.; Schiavone, E. J.; Mamontov, E.; Tyagi, M. Direct Measurement of Hydrogen Dislocation Pipe Diffusion in Deformed Polycrystalline Pd Using Quasielastic Neutron Scattering. *Phys. Rev. Lett.* **2014**, *113* (2), 025504. https://doi.org/10.1103/PhysRevLett.113.025504.
(25) Kruteva, M. Dynamics Studied by Quasielastic Neutron Scattering (QENS). *Adsorption* **2021**, *27* (5), 875–889. https://doi.org/10.1007/s10450-020-00295-4.
(26) Umesaki, N.; Iwamoto, N.; Tsunawaki, Y.; Ohno, H.; Furukawa, K. Self-Diffusion of Lithium, Sodium, Potassium and Fluorine in a Molten LiF + NaF + KF Eutectic Mixture. *J. Chem. Soc. Faraday Trans. 1 Phys. Chem. Condens. Phases* **1981**, *77* (1), 169. https://doi.org/10.1039/f19817700169.
(27) Lee, S.-C.; Zhai, Y.; Li, Z.; Walter, N. P.; Rose, M.; Heuser, B. J.; Z, Y. Comparative Studies of the Structural and Transport Properties of Molten Salt FLiNaK Using the Machine-Learned Neural Network and Reparametrized Classical Forcefields. *J. Phys. Chem. B* **2021**, *125* (37), 10562–10570. https://doi.org/10.1021/acs.jpcb.1c05608.
(28) Galashev, A. Y.; Rakhmanova, O. R.; Abramova, K. A.; Katin, K. P.; Maslov, M. M.; Tkacheva, O. Y.; Rudenko, A. V.; Kataev, A. A.; Zaikov, Y. P. Molecular Dynamics and Experimental Study of the

Effect of $CeF_3$ and $NdF_3$ Additives on the Physical Properties of FLiNaK. *J. Phys. Chem. B* **2023**, *127* (5), 1197–1208. https://doi.org/10.1021/acs.jpcb.2c06915.
(29) Zakiryanov, D. O. The FLiNaK-CeF3 Molten Mixture: A Comprehensive Structure Examination by Means of Ab Initio Molecular Dynamics. *J. Mol. Liq.* **2022**, *360*, 119400. https://doi.org/10.1016/j.molliq.2022.119400.
(30) Zakiryanov, D. The Physicochemical Properties of the $CeF_3$ – FLiNaK Molten Mixture: An *in Silico* Study. *Mol. Simul.* **2023**, *49* (8), 845–854. https://doi.org/10.1080/08927022.2023.2193656.
(31) Gardner, L.; Rose, M.; Cutrer, B. *Analytical Results for Prepared UIUC $F^7$LiNaK*; ANL/CFCT-21/46, 1838608, 172750; 2021; p ANL/CFCT-21/46, 1838608, 172750. https://doi.org/10.2172/1838608.
(32) Ehlers, G.; Podlesnyak, A. A.; Niedziela, J. L.; Iverson, E. B.; Sokol, P. E. The New Cold Neutron Chopper Spectrometer at the Spallation Neutron Source: Design and Performance. *Rev. Sci. Instrum.* **2011**, *82* (8), 085108. https://doi.org/10.1063/1.3626935.
(33) Walter, N. P.; Jaiswal, A.; Cai, Z.; Zhang, Y. LiquidLib: A Comprehensive Toolbox for Analyzing Classical and Ab Initio Molecular Dynamics Simulations of Liquids and Liquid-like Matter with Applications to Neutron Scattering Experiments. *Comput. Phys. Commun.* **2018**, *228*, 209–218. https://doi.org/10.1016/j.cpc.2018.03.005.
(34) Alvarez, F.; Alegra, A.; Colmenero, J. Relationship between the Time-Domain Kohlrausch-Williams-Watts and Frequency-Domain Havriliak-Negami Relaxation Functions. *Phys. Rev. B* **1991**, *44* (14), 7306–7312. https://doi.org/10.1103/PhysRevB.44.7306.
(35) Frandsen, B. A.; Nickerson, S. D.; Clark, A. D.; Solano, A.; Baral, R.; Williams, J.; Neuefeind, J.; Memmott, M. The Structure of Molten FLiNaK. *J. Nucl. Mater.* **2020**, *537*, 152219. https://doi.org/10.1016/j.jnucmat.2020.152219.
(36) Sprouster, D.; Zheng, G.; Lee, S.-C.; Olds, D.; Agca, C.; McFarlane, J.; Z, Y.; Khaykovich, B. Molecular Structure and Phase Equilibria of Molten Fluoride Salt with and without Dissolved Cesium: FLiNaK–CsF (5 Mol %). *ACS Appl. Energy Mater.* **2022**, *5* (7), 8067–8074. https://doi.org/10.1021/acsaem.2c00544.
(37) Jaiswal, A.; O'Keeffe, S.; Mills, R.; Podlesynak, A.; Ehlers, G.; Dmowski, W.; Lokshin, K.; Stevick, J.; Egami, T.; Zhang, Y. Onset of Cooperative Dynamics in an Equilibrium Glass-Forming Metallic Liquid. *J. Phys. Chem. B* **2016**, *120* (6), 1142–1148. https://doi.org/10.1021/acs.jpcb.5b11452.
(38) Sears, V. F. Neutron Scattering Lengths and Cross Sections. *Neutron News* **1992**, *3* (3), 26–37. https://doi.org/10.1080/10448639208218770.
(39) De Gennes, P. G. Liquid Dynamics and Inelastic Scattering of Neutrons. *Physica* **1959**, *25* (7–12), 825–839. https://doi.org/10.1016/0031-8914(59)90006-0.
(40) Embs, J. P.; Juranyi, F.; Hempelmann, R. Introduction to Quasielastic Neutron Scattering. **2010**. https://doi.org/10.3929/ETHZ-B-000023188.
(41) Arbe, A.; Colmenero, J.; Monkenbusch, M.; Richter, D. Dynamics of Glass-Forming Polymers: "Homogeneous" versus "Heterogeneous" Scenario. *Phys. Rev. Lett.* **1998**, *81* (3), 590–593. https://doi.org/10.1103/PhysRevLett.81.590.
(42) Toth, L. M. Coordination Effects on the Spectrum of Uranium(IV) in Molten Fluorides. *J. Phys. Chem.* **1971**, *75* (5), 631–636. https://doi.org/10.1021/j100675a006.
(43) Winner, N.; Williams, H.; Scarlat, R. O.; Asta, M. Ab-Initio Simulation Studies of Chromium Solvation in Molten Fluoride Salts. *J. Mol. Liq.* **2021**, *335*, 116351. https://doi.org/10.1016/j.molliq.2021.116351.
(44) Toth, L. M.; Boyd, G. E. Raman Spectra of Thorium(IV) Fluoride Complex Ions in Fluoride Melts. *J. Phys. Chem.* **1973**, *77* (22), 2654–2657. https://doi.org/10.1021/j100640a016.
(45) Dracopoulos, V.; Vagelatos, J.; Papatheodorou, G. N. Raman Spectroscopic Studies of Molten ZrF4–KF Mixtures and of A2ZrF6, A3ZrF7 (A = Li, K or Cs) Compounds. *J. Chem. Soc. Dalton Trans.* **2001**, No. 7, 1117–1122. https://doi.org/10.1039/b008433f.

(46) Walz, M.-M.; Van Der Spoel, D. Direct Link between Structure, Dynamics, and Thermodynamics in Molten Salts. *J. Phys. Chem. C* **2019**, *123* (42), 25596–25602. https://doi.org/10.1021/acs.jpcc.9b07756.
(47) Salanne, M.; Simon, C.; Groult, H.; Lantelme, F.; Goto, T.; Barhoun, A. Transport in Molten LiF–NaF–ZrF4 Mixtures: A Combined Computational and Experimental Approach. *J. Fluor. Chem.* **2009**, *130* (1), 61–66. https://doi.org/10.1016/j.jfluchem.2008.07.005.
(48) Rollet, A.-L.; Bessada, C. NMR Studies of Molten Salt and Room Temperature Ionic Liquids. In *Annual Reports on NMR Spectroscopy*; Elsevier, 2013; Vol. 78, pp 149–207. https://doi.org/10.1016/B978-0-12-404716-7.00004-3.
(49) Rollet, A.-L.; Bessada, C. Evidence of Dynamical Local Scale Distribution Heterogeneities in CsF-AF (A=Li, Na, K and Rb) Molten Salts. *J. Fluor. Chem.* **2015**, *180*, 40–44. https://doi.org/10.1016/j.jfluchem.2015.08.020.
(50) Sarou-Kanian, V.; Rollet, A.-L.; Salanne, M.; Simon, C.; Bessada, C.; Madden, P. A. Diffusion Coefficients and Local Structure in Basic Molten Fluorides: In Situ NMR Measurements and Molecular Dynamics Simulations. *Phys. Chem. Chem. Phys.* **2009**, *11* (48), 11501. https://doi.org/10.1039/b912532a.
(51) Bessada, C.; Rollet, A.-L. In Situ Spectroscopy in Molten Fluoride Salts. In *Molten Salts Chemistry*; Elsevier, 2013; pp 33–47. https://doi.org/10.1016/B978-0-12-398538-5.00003-2.
(52) Liu, Y.; Song, Y.; Ai, H.; Shen, M.; Liu, H.; Zhao, S.; Liu, Y.; Fei, Z.; Fu, X.; Cheng, J. Corrosion of Cr in Molten Salts with Different Fluoroacidity in the Presence of CrF3. *Corros. Sci.* **2020**, *169*, 108636. https://doi.org/10.1016/j.corsci.2020.108636.
(53) Langford, L.; Winner, N.; Hwang, A.; Williams, H.; Vergari, L.; Scarlat, R. O.; Asta, M. Constant-Potential Molecular Dynamics Simulations of Molten Salt Double Layers for FLiBe and FLiNaK. *J. Chem. Phys.* **2022**, *157* (9), 094705. https://doi.org/10.1063/5.0097697.
(54) Baes, C. F. A Polymer Model for BeF2 and SiO2 Melts. *J. Solid State Chem.* **1970**, *1* (2), 159–169. https://doi.org/10.1016/0022-4596(70)90008-3.
(55) Kergoat, M.; Massot, L.; Gibilaro, M.; Chamelot, P. Investigation on Fluoroacidity of Molten Fluorides Solutions in Relation with Mass Transport. *Electrochimica Acta* **2014**, *120*, 258–263. https://doi.org/10.1016/j.electacta.2013.12.035.
(56) Rodriguez, A.; Lam, S.; Hu, M. Thermodynamic and Transport Properties of LiF and FLiBe Molten Salts with Deep Learning Potentials. *ACS Appl. Mater. Interfaces* **2021**, *13* (46), 55367–55379. https://doi.org/10.1021/acsami.1c17942.